Princeton Plasma Physics Laboratory

PPPL- 5013

PPPL- 5013

Experimental Observation of 3-D, Impulsive Reconnection Events In A Laboratory Plasma

S. Dorfman, H. Ji, M. Yamada, J. Yoo, E. Lawrence,
C. Myers and T.D. Tharp

APRIL, 2014

PPPL PRINCETON PLASMA PHYSICS LABORATORY

Prepared for the U.S. Department of Energy under Contract DE-AC02-09CH11466.

Princeton Plasma Physics Laboratory
Report Disclaimers

Full Legal Disclaimer

Trademark Disclaimer

PPPL Report Availability

Princeton Plasma Physics Laboratory:

http://www.pppl.gov/techreports.cfm

Office of Scientific and Technical Information (OSTI):

http://www.osti.gov/bridge

Related Links:

U.S. Department of Energy

Office of Scientific and Technical Information

Fusion Links

Experimental observation of 3-D, impulsive reconnection events in a laboratory plasma

S. Dorfman, H. Ji, M. Yamada, J. Yoo, E. Lawrence, C. Myers, and T. D. Tharp
Center for Magnetic Self-Organization, Princeton Plasma Physics Laboratory, Princeton, New Jersey 08543, USA

(Received 4 November 2013; accepted 30 December 2013; published online 21 January 2014)

Fast, impulsive reconnection is commonly observed in laboratory, space, and astrophysical plasmas. In this work, impulsive, local, 3-D reconnection is identified for the first time in a laboratory current sheet. The two-fluid, impulsive reconnection events observed on the Magnetic Reconnection Experiment (MRX) [Yamada *et al.*, Phys Plasmas 4, 1936 (1997)] cannot be explained by 2-D models and are therefore fundamentally three-dimensional. Several signatures of flux ropes are identified with these events; 3-D high current density regions with O-point structure form during a slow buildup period that precedes a fast disruption of the reconnecting current layer. The observed drop in the reconnection current and spike in the reconnection rate during the disruption are due to ejection of these flux ropes from the layer. Underscoring the 3-D nature of the events, strong out-of-plane gradients in both the density and reconnecting magnetic field are found to play a key role in this process. Electromagnetic fluctuations in the lower hybrid frequency range are observed to peak at the disruption time; however, they are not the key physics responsible for the impulsive phenomena observed. Important features of the disruption dynamics cannot be explained by an anomalous resistivity model. An important discrepancy in the layer width and force balance between the collisionless regime of MRX and kinetic simulations is also revisited. The wider layers observed in MRX may be due to the formation of flux ropes with a wide range of sizes; consistent with this hypothesis, flux rope signatures are observed down to the smallest scales resolved by the diagnostics. Finally, a 3-D two-fluid model is proposed to explain how the observed out-of-plane variation may lead to a localized region of enhanced reconnection that spreads in the direction of the out-of-plane electron flow, ejecting flux ropes from the layer in a 3-D manner. © *2014 AIP Publishing LLC*. [http://dx.doi.org/10.1063/1.4862039]

I. INTRODUCTION

Magnetic reconnection is a fundamental plasma process involving the efficient conversion of magnetic field energy to plasma kinetic energy through changing field line topology. Reconnection has been observed in a variety of contexts[1] including tokamak plasmas,[2–4] the solar atmosphere,[5–7] and the Earth's magnetotail.[8,9] In all these cases, reconnection is not only fast, but also impulsive; in other words, a slow buildup phase is followed by a comparatively quick release of magnetic energy. Signatures of impulsive behavior have been previously identified in laboratory reconnection experiments.[10–12]

An open question in the literature is if this behavior can be described by a two-dimensional model with no spatial variation in the out-of-plane (y) direction or if impulsive reconnection is fundamentally three-dimensional. While two-dimensional, impulsive reconnection models exist, these models may be modified by the presence of a third dimension. For example, the reconnection rate spikes when secondary magnetic islands are ejected in 2-D simulations,[13] but in 3-D runs these islands become flux ropes with complex structure in the third dimension.[14] The addition of 3-D variation also allows for a large class of wave modes with finite k_y; these modes have long been considered as a possible source of anomalous resistivity that may speed up reconnection.[10,15–19]

In 2-D systems, there is a clear X-point where impulsive reconnection may take place, but in 3-D, fast reconnection could take place at all points along the X-line simultaneously or spread in the out-of-plane direction. Evidence for the later view is suggested by space measurements from both the magnetosphere and solar surface. In standard 2-D models of solar reconnection, the observed X ray emission from energetic electrons at the footpoints of a coronal loop moves outwards as successive field lines reconnect.[20] However, the observations show that there is a different pattern of emissions in select cases consistent with a 3-D spreading of the reconnection site along an arcade of neighboring loops.[21] In the magnetosphere, the distribution and time development of reconnection signatures in the out-of-plane direction also suggest a 3-D reconnection process.[22,23]

A large array of 3-D behaviors has also been observed in laboratory experiments. Experiments with a grid used to locally change the aspect ratio of the current sheet showed that 3-D tearing modes developed for large enough current sheet aspect ratios.[24] Newer experiments, involving the reconnection of externally generated flux ropes, also show a rich 3-D structure.[25,26] In previous work on the Magnetic Reconnection Experiment (MRX), magnetic fluctuations were sometimes observed in conjunction with two-fluid reconnection, suggesting an impulsive, 3-D picture.[12,27] On the Versatile Toroidal Facility (VTF), experiments with a strong guide field find that reconnection starts at one location and propagates in both directions around the torus[11] at the Alfvén speed. This is due to the presence of a global $m = 2$ or $m = 3$ mode in the device.

In contrast to the symmetric spreading found in the VTF experiments, when an equilibrium with zero guide field is set up in collisionless simulations such that reconnection is initialized in one location, the perturbation is often observed to spread asymmetrically in the third direction.[28,29] In the strong guide field case, simulations find that X-line spreading is due to bidirectional excitation of Alfvén waves while in the case with no guide field, the unidirectional spreading of the current carriers dominates.[30] The "reconnection wave" associated with this spreading in the zero guide field limit propagates in the direction of the current carriers and is driven by magnetic curvature in the electron frozen in region.[28] Similar Hall physics also describes the case of a density gradient in the electron flow direction within the current layer. In a 2-D Hall MHD picture with the outflow direction taken to be the symmetry direction, this may lead to magnetic shock like structures that rapidly thin the layer in the gradient region.[31,32]

3-D effects were previously identified as a leading candidate mechanism to explain an important discrepancy between MRX observations and 2-D particle-in-cell simulations. Specifically, the width of the electron diffusion region is consistently 3-5 times higher in MRX than in the simulations.[33] Since the width of the layer is related to the strength of the off-diagonal pressure terms in collisionless simulations, this discrepancy has important implications for the nature of the dissipation mechanism at the X-line. Prior investigations have focused on weak Coulomb collisions,[34] electromagnetic fluctuations,[35] and the influence of the probes used in the measurements, but a definitive answer remains elusive.

In this paper, localized current disruptions are identified in MRX as the first example of fast, impulsive, and *fundamentally three-dimensional* local magnetic reconnection in a laboratory current sheet. Signatures of flux ropes are found in the reconnecting current layer. The observed disruptions are due to the ejection of these 3-D, high current density regions associated with O-points at the measurement location. By contrast, magnetic fluctuations, long considered as a possible cause of anomalous resistivity, are not the key physics responsible for the observed impulsive phenomena.

The paper is organized as follows: Section II describes the experimental setup in MRX, including details of the discharge evolution and diagnostic setup. Section III describes the relationship between impulsive reconnection and the observed electromagnetic fluctuations. The detailed structure of the current layer during these impulsive events, including observed current disruptions and flux rope structures, is covered in Sec. IV. This is followed by Sec. V which details a qualitative 3-D, two-fluid picture that may explain the observations and explores the idea of small-scale flux ropes as a possible solution to the layer width discrepancy. Finally, concluding points are presented in Sec. VI.

II. EXPERIMENTAL SETUP

The experiments reported in this paper were conducted on MRX at the Princeton Plasma Physics Laboratory (PPPL).[36] MRX is a small laboratory device aimed at creating reconnection in a controlled setting where it can be studied in detail. The device is unique in that the details of the two-scale structure of the diffusion region may be resolved with little or no guide field, producing results that can be directly compared to the standard 2-D picture observed in simulations.[33,37,38] This allows for the present investigation in a real plasma on how the 2-D picture may be modified to produce the impulsive reconnection observed in real laboratory and astrophysical systems.

MRX is a cylindrical vacuum vessel with an inner radius of 76.2 cm and a 0.6 cm thick stainless steel wall; inside the vessel are two donut shaped flux cores of major radius 37.5 cm and minor radius 9.4 cm that produce the plasma and drive the reconnection. Each flux core consists of two windings, known as the Poloidal Field (PF) and Toroidal Field (TF) coils. A cutaway view of the machine showing the flux cores is shown in the left schematic of Fig. 1 along with the MRX coordinate system. Z is along the axis of the cylinder, R is radially outward, and θ is the out of plane coordinate around the cylinder: together these make up an R, θ, Z right handed cylindrical coordinate system. The experimental data presented primarily use the coordinates R, y, Z where R is the inflow direction, Z is the outflow direction, and y is a Cartesian coordinate locally oriented in the azimuthal direction in the small section of the device that most of the measurements are made. This region is illustrated in Fig. 2. Two probe setups are shown: one for measurements in the reconnection plane (left) and one to measure variation in the out-of-plane (y) direction (right). This approach differs significantly from Katz *et al.*[11] which models impulsive reconnection with a guide field as a global (i.e., periodic in the third direction) rather than a local phenomena. While global impulsive reconnection may be more applicable to tokamak sawteeth and reverse-field pinches where similar periodicity is observed,[3,39] the present study is more relevant to space and astrophysical plasmas which have no such periodicity.[40]

The current waveforms driven in the flux cores for a typical discharge are shown in Fig. 3. For this particular discharge, six 60 μF capacitors dump 10 kV into the PF windings at $t = 100\ \mu$s, leading to the vacuum field shown on the left side of Fig. 1. Once the PF current reaches its peak value at $t = 214\ \mu$s, four additional 60 μF capacitors are triggered, dumping 12 kV into

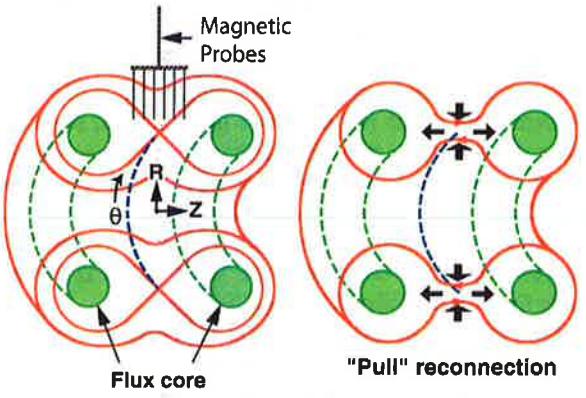

FIG. 1. Schematic of MRX operation and coordinate system. The left figure shows a cutaway view of the flux cores with the MRX coordinate system and a vacuum magnetic field. On the right is the configuration after the plasma has been created and the current in the flux cores begins to decrease: magnetic field lines that span both flux cores are pulled back in to reconnect in the central region.

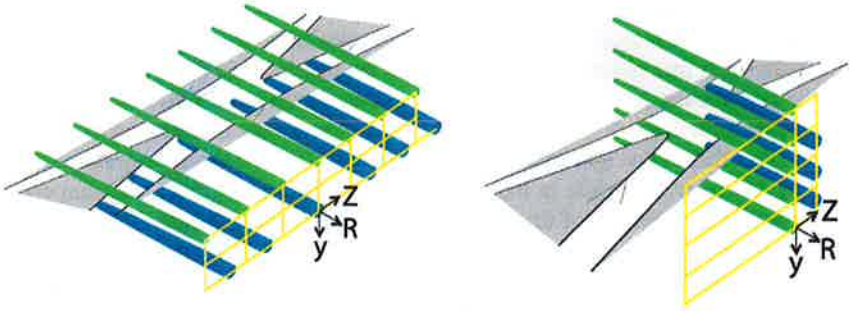

FIG. 2. Probe locations in the current sheet for in-plane measurements (left) and out-of-plane measurements (right). The local coordinate system is indicated by the coordinate axes in both plots. The Cartesian coordinate y is locally oriented in the azimuthal direction of MRX. For illustration purposes, parts of the reconnection plane are shaded gray. In the left panel, seven fine structure magnetic field probes (light green), each with 35 magnetic sensors, are located in the $y=0$ plane on both sides of the current sheet. In the right panel, five fine structure probes, each with 50 magnetic sensors, are located at $Z=0$, but at various out-of-plane y positions. Probes in both setups are separated by 3 cm. Additional probes to measure density, temperature, or high frequency magnetic field fluctuations may be placed nearby in the blue positions. Reprinted with permission from Dorfman *et al.*, Geophys. Res. Lett. **40**, 233 (2013).[42] Copyright 2012 American Geophysical Union. All Rights Reserved.

the TF windings. Plasma is then created ohmically, with higher density in the region near the flux cores where the inductive field produced by the TF windings is stronger.

Even though the PF current begins to decrease at $t=214\,\mu$s, the poloidal field does not respond to the pulling right away. The evolution is instead dominated by TF drive. Due to the plasma production process, there is excess density and B_θ magnetic field near the flux cores; this plasma and field pushes towards the X-point located at the vessel midplane. In the counter-helicity mode used in this work, the TF windings are connected such that the two flux cores produce opposite signs of B_θ. At the X-point, where the magnetic field is small, currents are driven in the plasma to prevent the inward motion of field in Z. In the region of this push current sheet, B_θ and B_R annihilate to produce B_Z and particle kinetic energy in what is known as the push phase of the discharge. This occurs during the time from $t\sim 260$–$300\,\mu$s, shaded in cyan in Fig. 3.

The focus of this work is on dynamics during the pull phase of the discharge from $t\sim 310$–$350\,\mu$s, shaded in green on Fig. 3. By this time, the PF current has significantly decreased, reducing the magnetic pressure by the flux cores; meanwhile, the ramp-up of the TF current stops. As a result, push reconnection stops, and poloidal magnetic field lines surrounding both flux cores reconnect, breaking in the center region and moving back into the cores on either side. This conversion of B_Z to B_R is shown in the right panel of Fig. 1. A current sheet forms and elongates in the central region to oppose the change in flux. At the time of the observed disruptions, typical plasma parameters are $n_e\sim 10^{13}/\text{cm}^3$ and $T_e\sim 5\,\text{eV}$. This gives a mean free path of 5 cm for electron-ion collisions, which is larger than the typical current sheet width of 1–2 cm; thus, the MRX layers at the disruption time are considered to be collisionless.

The dynamics of the pull phase of reconnection crucially depend on the initial conditions set by the push phase. In some discharges, B_θ has completely annihilated by the time pull reconnection starts, but more typically the push phase is slightly unbalanced, leading to a small left over negative guide field that is typically ~25% of the reconnecting field for the MRX operational mode used here. Furthermore, push reconnection does not occur symmetrically at all θ locations; as a result, the initial conditions for the pull phase may include the toroidal non-uniformities in density and field studied in Sec. IV C. This configuration is generated at the measurement location by operating the TF coils such that the toroidal field produced during the push phase is in the $-\theta$ direction on the $-Z$ side and the $+\theta$ direction on the $+Z$ side; this setup is termed "Case O" by Inomoto *et al.*[41] However, the precise push dynamics that create the non-uniformity are still a topic of active research; the present study takes the measured toroidal non-uniformities as an initial condition and explores the resulting pull reconnection dynamics.

III. ELECTROMAGNETIC FLUCTUATIONS

An appealing picture long considered as a candidate to explain fast reconnection is as follows: electromagnetic fluctuations generated by gradients in the reconnection region lead to additional terms in Ohm's Law at the center of the diffusion region.[43,44] Due to the correlation between fluctuating quantities, these terms enhance E/J, the effective

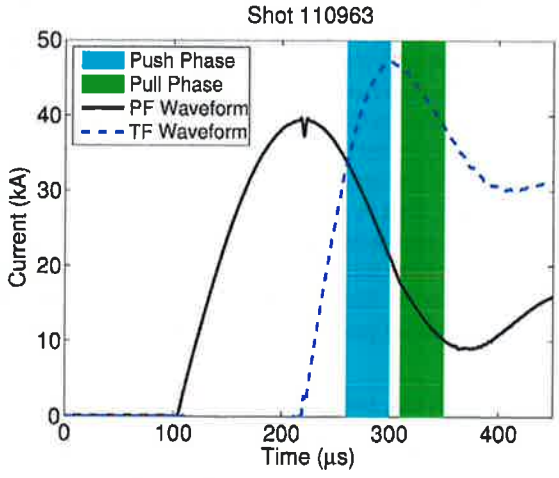

FIG. 3. Typical MRX flux core current waveforms for the present experiment. Shown as a function of time are the PF waveform (solid black), TF waveform (dashed blue), and cyan and light green shadings representing typical times for the push and pull phases of the discharge, respectively.

resistivity at the center of the diffusion region. Because the modes considered have finite k_y in the out-of-plane direction, this mechanism requires variation in all three spatial directions. A simple Sweet-Parker type analysis predicts that the additional dissipative terms from the fluctuations will enhance the observed reconnection rate. Therefore, a proposed model for an impulsive event is as follows: (1) reconnection starts slow, (2) fluctuations are generated due to gradients in the reconnection region, (3) dissipation is enhanced and reconnection speeds up, (4) the fluctuations relax the gradients and thus can no longer be driven, and finally (5) the reconnection rate returns to its slower classical value.

Previous work on MRX[10] showed a positive correlation between the fluctuation amplitude and the reconnection rate. While this result may be interpreted to support an anomalous resistivity model of fast reconnection, new detailed measurements of the fluctuation characteristics and layer structure (all completely consistent with Ji *et al.*[10]) reveal additional features that are not explained by this model. Furthermore, it is possible to show that if the observed modes have a phase velocity comparable to the electron drift velocity (as measured by Ji *et al.*[10] and Roytershteyn *et al.*[35]), the expected contribution to the force balance will be on the order of 1%. Following the same analysis as Ref. 10, the momentum per unit volume carried by the waves may be estimated as $k_y\mathcal{E}/\omega$, where $\mathcal{E} \approx 2|\tilde{B}|^2/8\pi$ is the total wave energy density. The contribution to the out-of-plane force balance of the electric field E_y^{wave} associated with the transfer of energy from electrons to the waves is then estimated; this force is given by the momentum per unit volume times twice the growth rate γ of the wave

$$enE_y^{wave} = 2k_y \frac{|\tilde{B}|^2}{8\pi}\frac{2\gamma}{\omega}. \quad (1)$$

Equation (1) with the assumption $\omega/k_y = v_{de}$ leads to an estimate of E_y^{wave} that is too small to explain the observed reconnection electric fields. Plugging $\omega/k_y = v_{de}$ into Eq. (1) with $v_{de} = (c/4\pi ne)(B_z^*/\delta)$ [B_z^* is measured at one layer width δ upstream] and assuming highly nonlinear waves with $\gamma \sim \omega$

$$E_y^{wave} = 2\frac{\omega}{c}\frac{\delta}{B_z^*}|\tilde{B}|^2. \quad (2)$$

Plugging in typical MRX parameters: $\delta \sim 1$ cm, $B_z^* \sim 150$ G and using a large fluctuation amplitude of $\tilde{B} \sim 5$ G at $\omega \sim 2\pi \times 2$ MHz, the resulting E_y^{wave} is only ~ 4 V/m, two orders of magnitude too small to explain the force balance in MRX. Note that this differs from the conclusion of Ji *et al.*;[10] this is because the product of the low density used in this previous estimate times the phase velocity of the observed modes is much smaller than the observed current density. In other words, for typical MRX parameters, there can only be a significant contribution to the force balance from the fluctuations for modes with a phase velocity significantly less than the electron drift speed. Consistent with this, 3-D simulation cases have been found with $\omega/k_y \ll v_{de}$ where fluctuations account for a portion of the force balance. These cases also have $T_e > T_i$ (Ref. 35) which is not usually true in the experiment.

Nonetheless, fluctuations are often found to be associated with impulsive behavior in the experiment. To illustrate this relationship, an example discharge is shown in Fig. 4. In the top panel of the figure, an impulsive event may be clearly identified during the time period between 330 and 335 μs. Key signatures include a drop in the out-of-plane current density J_y, a peak in the inductive electric field E_y, and large fluctuations at a nearby location. The bottom panel of the figure shows that the fluctuations occur when the current layer in black passes by the location of the fixed fluctuation probe in blue, consistent with previous MRX observations.[10,27] However, note that the fluctuations do not peak until the time that the inductive electric field E_y associated with the impulsive event peaks even though the current sheet crosses the exact location of the fluctuation probe 1 μs earlier. This is evidence that the timing of the fluctuations depends not only on the location of the current sheet but also on the timing of the impulsive event.

However, it is impossible to tell from Fig. 4 whether the fluctuations are a cause or a consequence of the impulsive event. In order to determine the answer to this question, a more in-depth look at current layer structure is necessary. This is covered in the following section.

IV. CURRENT LAYER DISRUPTIONS

A. Flux rope ejection

An example of what happens during a current disruption is shown in Fig. 5. The top time trace in panel A is the total out-of-plane current integrated over the field of view of the fine structure array in the left panel of Fig. 2. Plotted underneath is the inductive electric field at the X-point obtained through flux integration. The total out-of-plane

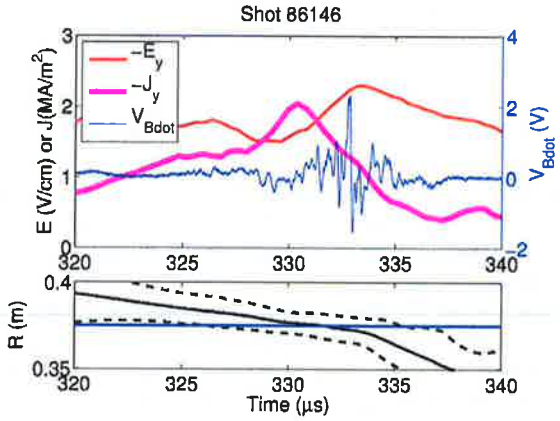

FIG. 4. Example showing the association of fluctuations with an impulsive reconnection event. Top panel: Inductive electric field E_y and current density J_y from fine structure probe measurements at $Z = -3$ cm, $y = 0$ and the raw magnetic fluctuation trace $\tilde{B}_z$ at $Z = -4.5$ cm, $y = 2.6$ cm. Bottom panel: Location of the current sheet (black trace), edge of the current sheet (black dashed trace), and location of the fluctuation probe (blue line). When an impulsive event (characterized by E_y peaking and J_y dropping) occurs, the fluctuations peak even though the layer center crosses the location of the fluctuation probe 1 μs earlier.

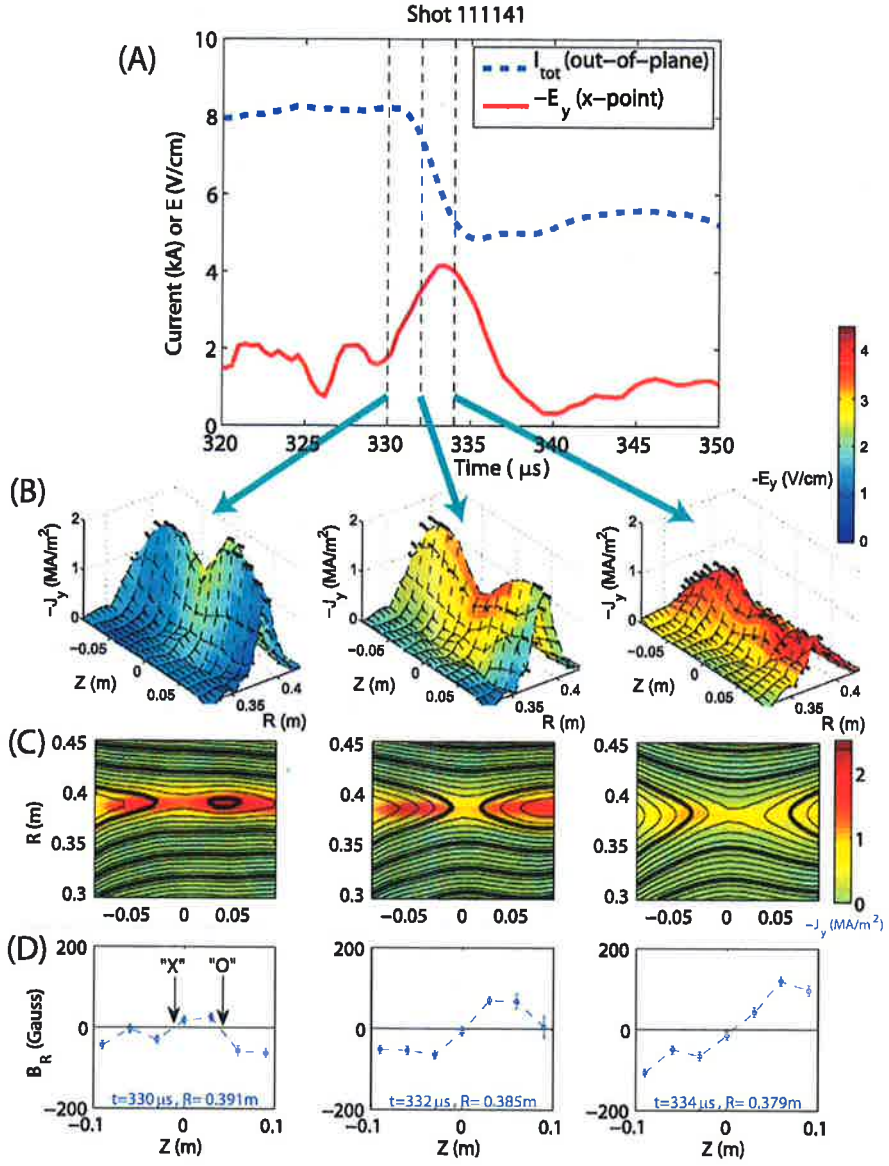

FIG. 5. An example of a current layer disruption in which the electric field peaks and the current drops as a flux rope structure is ejected from the layer. Row A: total out-of-plane current drop and reconnection rate enhancement during a current layer disruption. Shown are the total out-of-plane current integrated over the field of view of the fine structure array (thick dashed line) and inductive electric field at the X-point (solid line) for a representative deuterium discharge at 8 mTorr. Row B: detailed layer profiles from the fine structure magnetic field probes for the three times indicated by the vertical dashed lines in the top panel. The height of the contours represents out-of-plane current density $-J_y$ obtained though differentiation of 2-D magnetic field data, the color scale inductive electric field $-E_y$, and the arrows in-plane electron flow derived from the out-of-plane magnetic field. Row C: Flux plots with current density shaded for the same three times. Row D: B_R as a function of Z at the R location of the current sheet center as measured by the fine structure probe array. As the disruption proceeds, the layer aspect ratio decreases; at the same time, B_R increases, first near $Z=0$ and then at outer Z locations. An X and O-point for the first time slice are marked on the figure. Reprinted with permission from Dorfman *et al.*, Geophys. Res. Lett. **40**, 233 (2013). Copyright 2012 American Geophysical Union. All Rights Reserved.

current is initially 8 kA, but drops by 3 kA within about 4 μs around $t=332\,\mu$s. This timescale for the out-of-plane current drop is comparable to an ion cyclotron time of $\sim 4\,\mu$s obtained from the shoulder field of a Harris fit to the magnetic profile at $t=332\,\mu$s. At the same time, the electric field rises from 2 V/cm to over 4 V/cm as the reconnection rate spikes.

The details of the layer structure for this discharge reveal that the disruption is due to the ejection of current density from the layer. Each of the three times in panel B of Fig. 5 represents one of the times indicated by the vertical dashed lines in panel A. The changing height of the contours between panels represents the out-of-plane current density moving outward in Z over the course of the disruption. Meanwhile, the reconnection electric field E_y, indicated by the color code, initially peaks at the layer center and then also spreads outwards in Z. The arrows show the electron outflow $-J_z$ inferred from B_y measurements; J_z peaks around the disruption time.

The areas of high current density which peak downstream from the layer center have an O-point structure as illustrated by the flux plot and B_R measurements shown in panels C and D of Fig. 5 for each of the times in panel A. At $t=330\,\mu$s, just before the total current begins to drop, B_R as a function of Z at the R location of the X-point shows two clear zero crossings, identified as the X and O-points on the figure. Consistent with this, the corresponding flux plot clearly shows the O-point associated with the flux rope structure. A third zero crossing is not well resolved, but suggests a possible second flux rope at $-Z$. To avoid confusion with the various definitions of flux ropes that appear in the literature, a "flux rope" is defined here as a 3-D, high current density region associated with an O-point at the measurement location. Inside a flux rope, an enhanced core field may be observed. When the four density measurements per discharge are aligned along Z at the radial location of the flux rope, density is also observed to peak inside the structure. Since these additional signatures are not always clear, it is

important to note that the definition presented here differs from the most rigorous definitions of a flux rope (e.g., NRC[45]) found in the literature.

The B_R profiles at the current sheet center are consistent with the picture of flux ropes moving outward in Z. Because the initial E_y peak at $t = 330\ \mu s$ in panel (B) of Fig. 5 is localized near the X-point, there will be finite $\partial E_y/\partial z$ and hence $\partial B_R/\partial t$ associated with this spatial structure. This time derivative has the effect of increasing the slope of B_R near the X-point; this change in slope is clear from a comparison of the left and center portions of panel (D) of Fig. 5. As the slope of B_R changes and the flux rope moves away from the X-point, the fast reconnection region spreads outwards, and so does the spatial derivative of E_y. Thus, by the time shown in the right portion of panel (D), the slope of B_R has also increased at large $|Z|$; consistent with this, the initially elongated layer decreases in aspect ratio as the flux rope is ejected.

B. Buildup of current density

A disruption occurs following a slow buildup phase; during this buildup period, the discharge transitions from the collisional to the collisionless regime; meanwhile, current density slowly builds up due to collisionless effects. This is shown in Fig. 6 which plots three parameters related to the collisionality regime in the top section and the out-of-plane current density J_y at $Z = 3$ cm in the bottom section. Only shots with a clear current disruption within the range of the fine structure probes are selected for this average plot using the criteria outlined in the figure caption. These criteria are met in 112 out of 315 discharges, a bit more than one-third

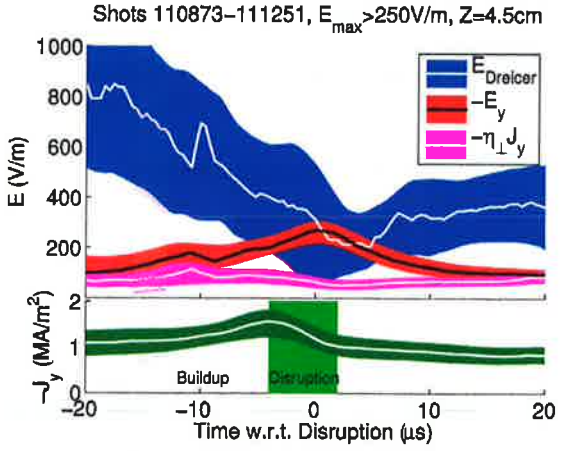

FIG. 6. Plots showing the transition from collisional to collisionless regimes that occurs during the current density buildup phase. Top plot: Inductive electric field (red), runaway electric field (blue), and $\eta_\perp J_y$ (magenta) at the location of the in-plane magnetic null. Bottom plot: current density as a function of time showing a slow $\sim 15\ \mu s$ buildup and a fast $\sim 5\ \mu s$ disruption phase; the disruption phase is represented by the shaded green region. Magnetic measurements are from a fine structure probe at $Z = 3$ cm; density and temperature are from a Langmuir Probe at $Z = 4.5$ cm. Error bars representing an average over 112 deuterium discharges at 8.1 mTorr are smoothed over 4 μs and represented by shaded regions. The discharges selected all have a peak electric field at the X-point greater than 250 V/m between 325 μs and 335 μs at a radial location between 37 cm and 39 cm.

of the cases checked. The data are plotted with respect to the disruption time which is defined as the time at which the inductive electric field at the X-point peaks. The current density trace shows an $\sim 15\ \mu s$ buildup phase during which the current density increases by 50% and a comparatively fast disruption phase lasting only $\sim 5\ \mu s$ during which the current density decreases back to its initial value. Note that the increase in current density is due to a narrowing of the layer width rather than an increase in the total current. This is consistent with Fig. 5 which shows no increase in the total current prior to a disruption.

The top half of Fig. 6 illustrates the collisional to collisionless transition that occurs during the buildup phase. Values of the inductive electric field E, the runaway electric field $E_{Dreicer}$ ($E_{Dreicer} \equiv \sqrt{T_e m_e}\nu_e/e$), and the resistive contribution to the force balance $\eta_\perp J_y$ during the buildup and subsequent disruption are shown in the top plot. $E_{Dreicer}$ and $\eta_\perp$ are calculated using density and temperature measured by a fixed Langmuir probe at $Z = 4.5$ cm. The probe is scanned every 1 cm in R between discharges to obtain the average profiles. Density and temperature at the magnetic field reversal location are obtained by interpolating these averages. Early in the buildup phase, $E_{Dreicer}$ is considerably greater than E_y and $\eta_\perp J_y$ is within errorbar of E_y, indicating that reconnection is collisional. However, by the start of the disruption phase, E_y and $E_{Dreicer}$ are equal to within errorbar and $\eta_\perp J_y$ is small; the slow $\sim 15\ \mu s$ timescale for these changes suggests that a gradual transition to collisionless regimes occurs during the buildup phase that precedes a disruption. This behavior is in direct contrast to 2-D models, such as the one by Cassak *et al.*[46] in which a fast collisional to collisionless transition causes impulsive phenomena.

Note that since $E_{Dreicer} \sim n/T_e$, and T_e changes by only a few eV, the decrease in $E_{Dreicer}$ over time is mainly due to the depletion of upstream density. This is shown explicitly in the left panels of Fig. 7 which shows the average density profiles from the radial Langmuir probe scan for three of the times in Fig. 6: during buildup, just before the disruption, and during the disruption. The data reveal the primary reason for the trend in $E_{Dreicer}$: during the buildup phase, the upstream density is gradually depleted as plasma enters the layer and is ejected into the outflow region. By $t = 0$, the density profile at the X-point to the left of the high current density region is essentially flat in the radial direction. In other words, the disruption occurs as the reconnection layer "runs out" of upstream density. Note that even as the average density is decreasing from -10 to $-5\ \mu s$, the current density in the right panels of Fig. 7 is building up; as seen in Fig. 6, the speed of the increase is especially pronounced towards the end of the buildup phase when the layer is collisionless. This suggests that the mechanism directly responsible for the buildup operates in the two-fluid regime. Other signatures of the buildup phase consistent with these features include an increase in the magnitude of the observed out-of-plane quadrupole magnetic field, enhanced toroidal field inside the flux rope, and possible electron heating in the flux rope region. Note, however, that this does not imply that the collisional to collisionless transition is the disruption mechanism. 2-D kinetic simulations (modeled after Ref. 47) in which such a

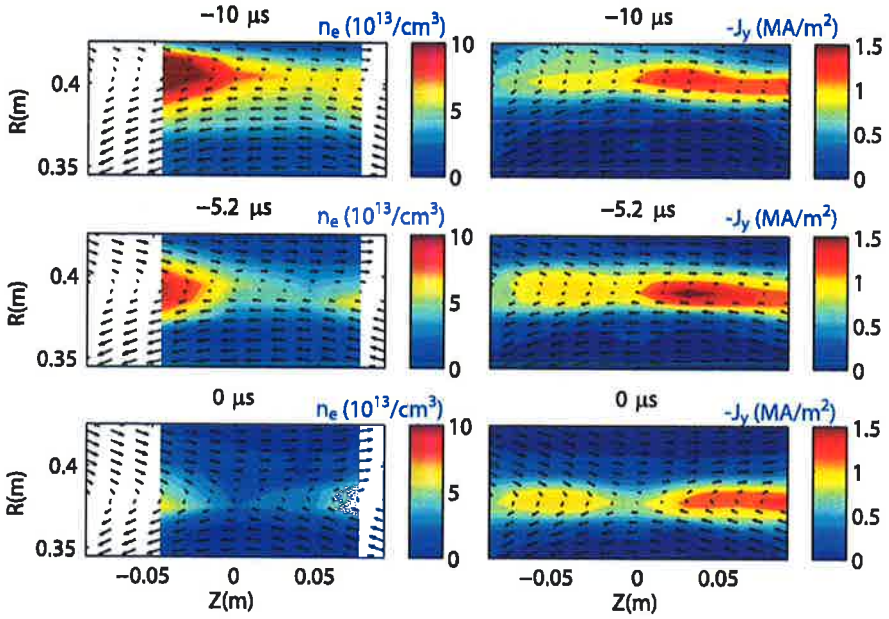

FIG. 7. A 2-D in-plane view of density depletion and current density buildup/ejection. Density (n_e) and current density (J_y) as a function of time with respect to the disruption time at t = 0 μs are shown for an average of the same 112 deuterium discharges used to construct Fig. 6. Three times from Fig. 6 are shown from top to bottom: during buildup, just before the disruption, and during the disruption. Density is measured with Langmuir probes at $Z = -4.5$, 0, 4.5, and 7.5 cm scanned every 1 cm between shots. Magnetic field is measured using fine structure probes placed every 3 cm in Z. As time advances towards the disruption, upstream density is depleted by reconnection.

transition occurs do not disrupt despite similar density profile evolution to the experiment.

Although the buildup mechanism is collisionless, the depletion of upstream density associated with the transition to collisionless regimes still plays an important role. This conclusion may be deduced from an examination of discharges that do not transition. For example, when density remains high and $E/E_{Dreicer}$ remains low, the current density does not vary much in time and there is no disruption. But when reconnection is entirely two-fluid ($E/E_{Dreicer}$ and current density start high), small impulsive events are observed rather than a single dramatic disruption; a good example of this case is the right half of Fig. 13. This further implies that a collisionless 3-D mechanism is responsible for the impulsive behavior observed.

C. Out of plane measurements

Strong gradients of equilibrium quantities in the y direction are routinely observed in disruptive discharges, underscoring the 3-D nature of the phenomena. An example is shown in the left panel of Fig. 8 for the density at the center of the layer and the shoulder magnetic field B_{sh} from a Harris fit at a time near the start of the main pull reconnection phase. The center panel shows the same quantities near the disruption time when the magnetic field gradient is in the process of relaxing. At this time, the plasma density has decreased; in other words, the depletion of upstream density observed in Fig. 7 translates into the flattening of the y density gradient in Fig. 8. Note that the density measurements are an average over discharges at a Z location near the typical location of the X-point; within a single discharge, as described in Sec. IV A, the density often remains high inside the flux rope region. In the far right panel of Fig. 8, density and magnetic field are displayed towards the end of the pull reconnection period by which time the original B_{sh} gradient is gone. As with the in-plane measurements, discharges with a clear disruption are selected using the thresholds explained in the figure caption.

To fully understand the key role out-of-plane gradients play in a current disruption, it is important to examine the detailed time evolution of the y gradients in B_{sh} during both the buildup and disruption phases of the discharge. The time evolution of the magnetic field profile in the R-y plane is shown for an example discharge in Fig. 9. The first column of plots shows the buildup phase with time increasing downwards; the green region where the magnetic field is small visibly narrows, especially at smaller y, indicating an increase in the current density. The second column of plots shows the disruption phase; the green region broadens, first at small y by $t = 331.6$ μs and then at large y by $t = 333.2$ μs. Therefore, the disruption process is not uniform in y, but instead spreads in the electron flow (positive y) direction.

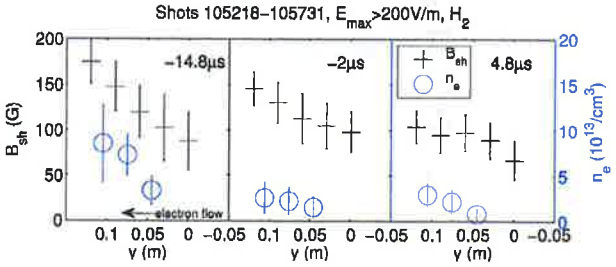

FIG. 8. Probe measurements of out-of-plane gradients before a current layer disruption and prior to flux rope formation (left), during the disruption (center), and after the disruption (right). Black crosses represent the upstream magnetic field obtained from fitting the experimental data to a Harris profile[48] in the inflow region at $Z = 0$. Blue circles show density measured at the current sheet center at $Z = 2.6$ cm. Data are averaged over 101 10.8 mTorr hydrogen discharges with a peak inductive electric field of at least 200 V/m at $y = 6$ cm. The time indicated in the upper portion of each panel is with respect to the disruption time. In the pull phase initial condition, there are strong gradients in both quantities in the out-of-plane electron flow (+y) direction. Following the disruption, the original magnetic field gradient has relaxed and density is lower. During the disruption, there is no density gradient and the magnetic field gradient is in the process of relaxing.

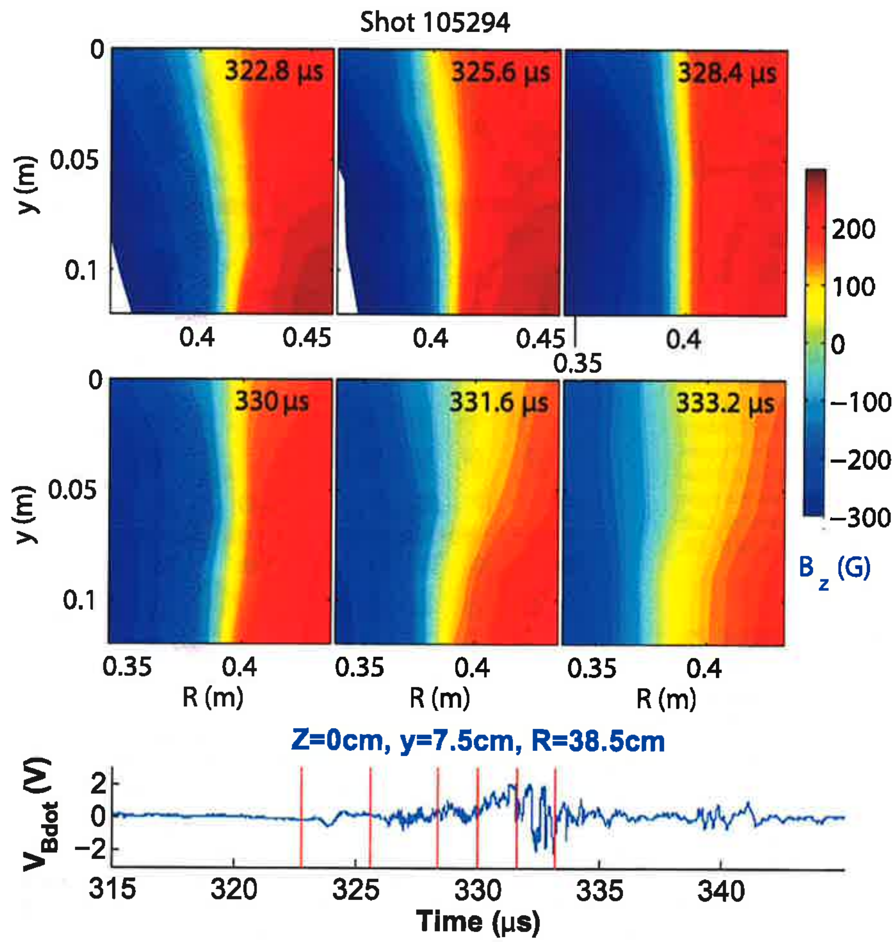

FIG. 9. Out-of-plane view of current density increase and subsequent disruption. Magnetic field B_z is plotted at six times as a function of R and y for an 8.5 mTorr deuterium discharge. The top row shows the buildup phase with time increasing to the right while the second row shows the disruption. Note that the disruption spreads from top to bottom in the electron flow ($+y$) direction. Also shown in the bottom panel of the figure is a plot of magnetic fluctuations measured at $Z=0$ cm, $y=7.5$ cm, $R=38.5$ cm with the six times for the upper plots indicated by vertical red lines. Reprinted with permission from Dorfman *et al.*, Geophys. Res. Lett. **40**, 233 (2013). Copyright 2012 American Geophysical Union. All Rights Reserved.

The time evolution of the y gradients of B_z is related to the flux rope structures observed in the in-plane measurements. When a flux rope builds up at or passes by the location of the probes stacked at $Z=0$, the layer narrows. Once the flux rope is ejected past the Z location of the stacked probes, the layer is seen to broaden and disrupt. The region in which this buildup occurs is characterized by a density gradient in the electron flow ($+y$) direction as seen, for example, in the initial state of Fig. 8.

V. DISCUSSION

While 3-D flux ropes are analogous to 2-D islands, several key features of the observed current disruptions have no clear 2-D analogue. For example, strong out-of-plane gradients are consistently observed in disruptive discharges; this association cannot be explained by a 2-D model. Similarly, the spreading of the disruption in the y direction requires 3-D physics to explain. Finally, magnetic fluctuations in the lower hybrid frequency range with finite k_y are observed concurrently with disruptions (see, for example, the bottom panel of Fig. 9). Although these fluctuations have characteristics consistent with Ji *et al.*,[10] the observed out-of-plane gradients and flux rope structures are not predicted by a picture in which small-scale fluctuations are responsible for a locally enhanced reconnection rate. Therefore, neither a 2-D model nor an anomalous resistivity model is capable of explaining the observations. The key features of the disruption imply a fundamentally three-dimensional process.

A. 3-D, two-fluid picture

This raises an important question: How do these 3-D features lead to the observed disruptions? While this is still a subject of active research, with some physical intuition it is possible to construct a simplified model consistent with the observations. This 3-D two-fluid model builds on the picture of impulsive two-fluid dynamics developed by Yamada.[12] Due to the two-scale structure of the diffusion region, there is a region where only electrons are frozen to the field and Hall MHD applies. Here, electrons and magnetic field move together while the slower ions control plasma density. The resulting magnetic field configuration is schematically illustrated on the left side of Fig. 10 from Yamada[12] which shows this frozen-in electron flow stretching magnetic field lines out of the reconnection plane in the y direction. Note that a Cartesian coordinate system is employed with x as the inflow direction and z as the outflow direction. The right panel of the figure shows B_z magnetic field and electron flow vectors for a cut in inflow region (x-y plane) near the X-point at $z=0$; note that this picture assumes that there is no y variation of the field or flow. Frozen in electrons convect the magnetic field in both the x and y directions towards the red dissipation region at $x=0$ where reconnection takes place.

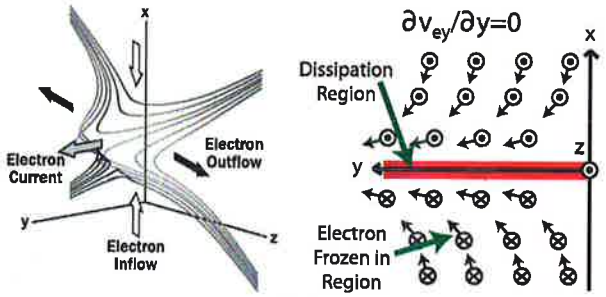

FIG. 10. Schematic from Yamada[12] showing electrons convecting the magnetic field lines out-of-plane (left) and a cut of this schematic in the inflow direction at $z=0$ near the X-point (right). For the figure on the right, circles represent magnetic field B_z and arrows represent frozen in electron flow for the portion of the inflow region (x-y plane) near the X-point ($z=0$) where electrons are frozen to the field lines. The horizontal red line at $x=0$ represents the electron dissipation region. Note that the figure on the left illustrates 2-D features of what could be a 3-D system; the figure on the right assumes a 2-D picture with no variation in the out-of-plane direction. Left panel reprinted with permission from M. Yamada, Phys. Plasmas **18**, 111212 (2011). Copyright 2011 American Institute of Physics.

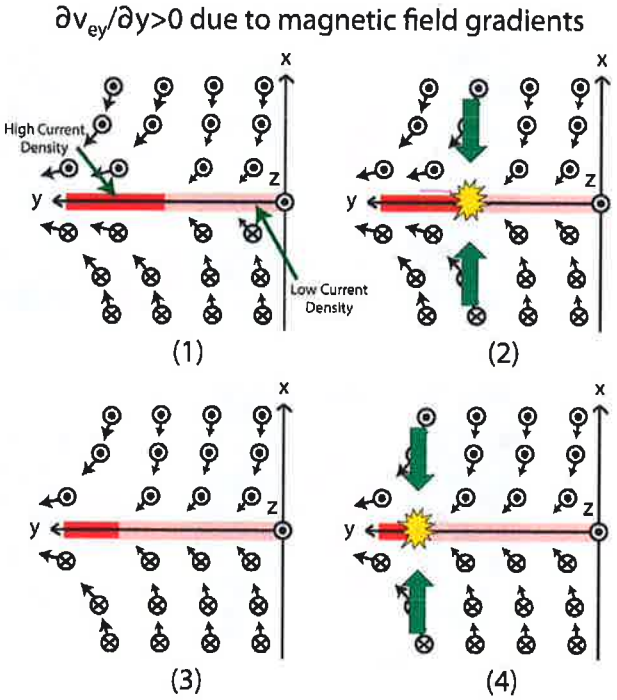

FIG. 11. Diagram showing how a disruption may spread in y when $\partial v_{ey}/\partial y > 0$ due to magnetic field gradients associated with y variation of B_x. B_x is not shown explicitly, but the resulting modifications to the flow pattern and current density in the 3-D case are. For example, lighter shading represents lower current density in the dissipation region due to larger $\partial B_x/\partial z$. The reconnection rate is enhanced in the gradient region of panel (1) by the mechanism described in the text. This enhanced reconnection, indicated by the large arrows in panel (2), leads to B_x generation which decreases v_{ey}. The gradient then moves in the $+y$ direction and the disruption spreads, as shown in panels (3) and (4), respectively.

The reconnection electric field E_y is primarily balanced by the Hall term in the electron frozen in (two-fluid) region and balanced by the dissipation term in the red dissipation region. In Yamada,[12] it was shown that the electron flows associated with Hall dynamics fluctuate in time leading to impulsive reconnection. This time-dependence may be due to 3-D dynamics.

Consider, for example, how the simple picture of bent field lines in Fig. 10 behaves in the presence of y gradients in v_{ey} associated with the out-of-plane density and magnetic field gradients. These gradients, which are present at the start of pull phase in disruptive discharges, play a key role in the discharge evolution. The simplest possible overview of the proposed physical picture leading to a disruption in MRX is as follows: The density gradient controlled by the heavier ions holds the magnetic field gradients and lighter electrons in place. Current density builds up until the plasma density upstream from the X-point is sufficiently depleted by slow reconnection. Once the out-of-plane density gradient flattens at the X-point, the out-of-plane magnetic field gradients can no longer be held in place, and the layer disrupts over a fast timescale.

To understand how this corresponds to the physical picture in Fig. 10, first consider a simplified version of the situation that exists in the inflow region just before a disruption. Out-of-plane density variation is negligible and only the remaining out-of-plane magnetic field gradients are considered. For both simplicity and consistency with the picture of bent field lines in Fig. 10, the gradients considered are due to y variation of B_x (see the caption of Fig. 11 for details). The four different panels of Fig. 11 describe the time sequence of how a disruption may occur and spread in the y direction:

1. **Net flux of electrons and field out of the y gradient region due to y flows:** On the left side of panel (1) at large y, the current density is higher as indicated by the darker red color of the dissipation region. Consistent with this, the two rows of field lines at large y are convected by the electrons in y faster than the two rows at small y. As a result of the difference in v_{ey} between the two regions, there will be a net flux of field lines out of the y gradient region due to y flows, but only at x locations well described by Hall physics. This is illustrated by the shape of the white gap between the fast and slow moving electrons in panel (1) which shows that in the region of the y gradient, the net y flux $\Delta v_{ey} B_z$ is highest at the x locations closer to the edge of the dissipation region and zero near the outer edge of the two-fluid region. The latter condition is dictated by the outer boundary: far outside of the current sheet where the heavier ions are also tied to the field, there can be no displacement of field due to electrons alone.
2. **Disruption in the gradient region:** Even as electrons and field lines are depleted at the inner x locations along the y gradient, there is still a plentiful supply of field at nearby x locations on the outer side of the electron frozen in region. Under the charge neutrality assumption, electron flow continuity in the Hall MHD region demands that a nonzero and positive $\partial v_{ey}/\partial y$ be supported by an enhanced inflow of electrons and field from the outer edge of the Hall MHD region as indicated by the thick green arrows in panel (2). The enhanced inflow of electrons and field lines in the x direction increases the local reconnection rate in the orange region of panel (2), causing the layer to disrupt at this y location. From a force

balance perspective, as the electron inflow in the two-fluid region increases, the Hall contribution to E_y is enhanced. Therefore, dissipation in the orange portion of the dissipation region must increase in order to maintain force balance in the y direction. If the dissipation is due to the off-diagonal pressure tensor terms, the additional electrons entering the diffusion region through increased v_{ex} will increase the magnitude of the off-diagonal terms self-consistently with the v_{ex} enhancement. As the additional electrons must exit the diffusion region through the outflow, v_{ez} should also increase; therefore, an overall increase in the magnitude of the Hall effects and the dissipation terms are expected in the fast reconnection region.

3. **Gradient region moves in $+y$:** The enhanced reconnection region associated with the disruption in panel (2) will lead to a quick conversion of reconnecting field B_z to reconnected field B_x. This change in the layer structure reduces v_{ey} in the gradient region, modifying the electron flow pattern to that shown in panel (3) of the figure. The structure of the red dissipation region adjusts as necessary; this is indicated by the spread of the light color, low current density portion to the left in panel (3).
4. **Disruption spreads in $+y$:** The process illustrated by panel (2) repeats at the new location of the y gradient and the disruption spreads!

This proposed physical picture of the disruption may equivalently describe the propagation of the "reconnection wave" outlined by Huba and Rudakov.[28,29,31,32] In this case, the magnetic field perturbation that creates the v_{ey} gradients associated with bent field lines is externally imposed rather than generated by pre-existing magnetic field gradients. Also note that if the v_{ey} gradient is in opposite direction from the case shown in Fig. 11, the spreading perturbation may sharpen rather than weaken the layer.

Several key features of the proposed model agree well with MRX observations. For example, the model explains the observed peak in the reconnection rate, the disruption spreading in y, and the importance of the out-of-plane magnetic field gradient in the initial condition. Consistent with Yamada *et al.*,[1] the enhanced inflow described by the model means that the Hall signatures will peak at the disruption time; measurements of the quadrupole magnetic field and electrostatic potential well (not shown) corroborate this prediction. Although the observed flux ropes are not explicitly included in the model discussed here, note that the cut in Fig. 11 is taken at the Z location of the X-point. As the reconnection rate at the X-point peaks at a given y location, any flux ropes that have formed to the side of the X-point will necessarily be ejected outward, consistent with the picture of Fig. 5. This ejection process causes the gross magnetic topology change in rows B and C of the figure that makes the disruption rather dramatic.

Flux rope formation is possibly related to the initial state described by the left panel of Fig. 8. Here, both density and magnetic field gradients are present with similar scale lengths. In this case, the v_{ey} gradients will be dominated by the density variation held in place by the heavier ions, leading to the picture shown in Fig. 12 with $\partial v_{ey}/\partial y < 0$. Note that the electron dissipation region shading is lighter at small y; even though v_{ey} is greater in this region, the current density is smaller due to the lower plasma density. There is now a net flux of electrons and field from the y direction into the y gradient region at the x locations closest to the dissipation region. Therefore, to maintain charge neutrality, the continuity equation predicts that v_{ex} is reduced and reconnection slows. Consistent with this, B_z is enhanced and B_x is reduced, leading to a buildup of current density. Note that this buildup is associated with the lighter electrons, but the gradient is held in place by the heavier ions which evolve over slower timescales. Therefore, unlike the picture in Fig. 11 where the change in the reconnection rate causes the field gradient region to move, the density gradient remains in place, and current density may continue to build up. The elongated layers that result from this process may be tearing unstable, possibly contributing to the formation of flux rope structures. This buildup process ends when upstream density is depleted and the y density gradient at the X-point next to the flux ropes flattens; the remaining magnetic field gradients then dominate v_{ey}, potentially leading to the disruption process described above.

B. Small scale flux ropes: A solution to the layer width discrepancy?

The flux ropes ejected during a disruption may provide an important clue towards the solution of the layer width discrepancy between MRX and kinetic simulations. But these observable flux ropes alone cannot explain the discrepancy; while the layer may be broader in the flux rope region, the layer should be able to thin to ρ_e scales in other portions of the current layer if no other structure is present. However, large scale current layer disruptions are not the only kind of impulsive event observed.

Small impulsive events are also observed which are associated with less dramatic peaks in E_y and a flat B_R profile with no observable flux ropes. An example case is shown in Fig. 13. The left side of the figure is reprinted from Fig. 5; the time evolution of the out-of-plane current and inductive electric field in the upper left shows clear disruptive

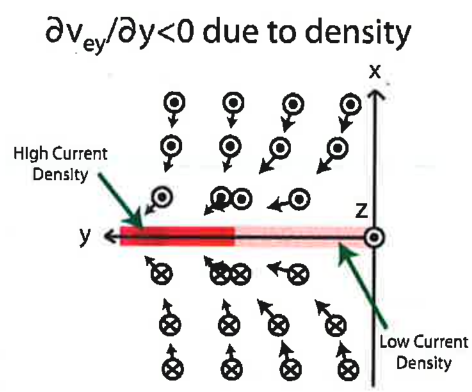

FIG. 12. Diagram showing how current density may build up in the y gradient region when $\partial v_{ey}/\partial y < 0$ due to density gradients. The buildup is due to a reduction in the reconnection rate in the gradient region by the mechanism described in the text.

behavior. Taking a cut of B_R as a function of Z at the layer center just before the current drops, clear X and O-points are observed. By contrast, the discharge on the right displays multiple small peaks in the inductive electric field and multiple small current drops. Just before one of these drops, an examination of B_R as a function of Z at the layer center reveals a region where B_R hovers near zero, possibly indicating the presence of small scale flux ropes below the probe resolution.

Therefore, an intriguing possibility is that these small impulsive events are simply miniature versions of large scale disruptions. If this is the case, collisionless layers in MRX may be unstable to the formation of small scale flux ropes before the layer can thin down to ρ_e scales; these small flux ropes could then be responsible for the wider electron layers observed in the experiment. Note that under this scenario, flux ropes would not be observed until they grow to a size that can be resolved by the diagnostics. If this is the case, the high current density observed in the outflow region (not shown) in the discharge on the right side of Fig. 13 could be the result of the continual impulsive ejection of these structures from the layer center.

Evidence to support the presence of small scale flux ropes is displayed in Fig. 14 which shows a distribution of flux rope sizes for a set of 315 discharges. For each event, the time averaged Z scale of the flux rope, as defined by the distance between the X and O line crossings, is plotted. Events are observed by the fine structure probe array which has a maximum Z resolution of 3 cm; the data are then interpolated onto a grid of resolution 1.5 cm and the zero crossing points are found. The result is consistent with an exponentially decreasing distribution starting near the smallest scale resolved by the probe array and ending at the largest scale measured; this range is represented by the gray shaded region. As explained in the figure caption, there is a gradual transition from white (poorly resolved) to gray (fully resolved) shading in the figure. The data suggest that flux ropes of all sizes may be present, but are not always resolved by the probes. This conclusion is consistent with data reported in Dorfman[49] from a fixed B_R probe with finer-scale resolution.

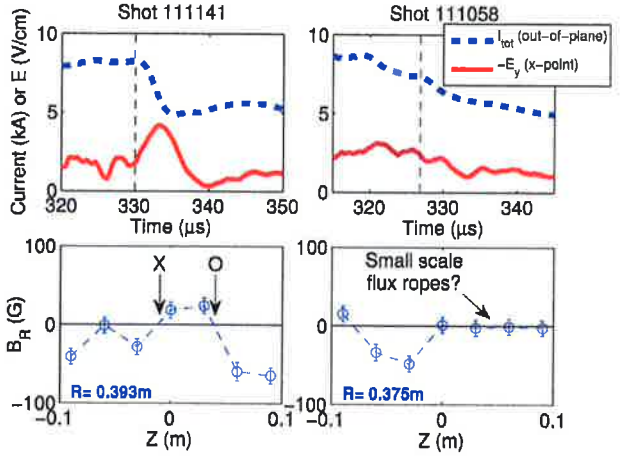

FIG. 13. Comparison of large and small impulsive events. The top panels show the total out-of-plane current integrated over the field of view of the fine structure probes and the inductive electric field measured at the X-point. The reconnected electric field B_R is displayed as a function of Z in the bottom panel at the time indicated by the vertical dashed line in the corresponding top panel. The discharge on the left illustrates the case of a large impulsive event associated with a clear X and O-point. To the right is an example case with multiple small impulsive events and possible flux ropes below the probe resolution.

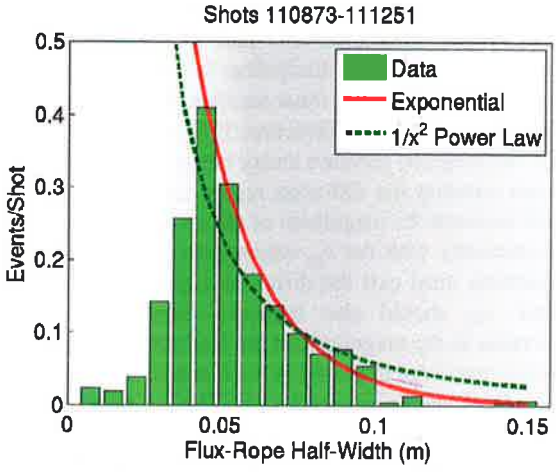

FIG. 14. Statistical distribution of flux rope half widths in the Z direction for a set of 315 deuterium discharges as measured by the fine structure probes at $y=0$ and the R location of the current sheet center. For each event, the average half-width over the lifetime of the flux rope is determined by measuring the distance between X and O line crossings in the B_R profile. A statistical distribution of events is presented in bar form and normalized to the number of shots. The scale length for the exponential curve overplotted is 2.2 cm. The fine structure probes have a maximum resolution of 3 cm and a range of 18 cm centered at $Z=0$. The gray shaded region represents the range of flux rope sizes that can be resolved under these measurement constraints. Depending on the position of the X and O line crossings relative to the probe coils, some events with half-width less than twice the probe resolution (or 6 cm) will not be fully resolved; hence, the gradient shading between 3 cm and 6 cm on the plot. Similar gradient shading is used for sizes bigger than half the probe range.

This picture suggests that flux ropes form at small scales and then may grow and merge to large scales before their ejection from the layer. While this is similar to the conclusion reached by several previous numerical and analytical studies,[50–53] it is important to note that the exponential distribution reported here cannot be easily compared to all distributions previously reported in the literature. Specifically, some references express the size distribution in terms of the peak flux ψ in the island or flux rope.[50,53] Since this peak value may fall between two measurement coils in the experiment, no comparable experimental figure can be produced. However, other studies also predict a distribution in terms of the scale size of the island or flux rope;[51,52] these results are easier to compare with the experiments.

A comparison between two models and the experiment is shown in Fig. 14. The solid curve is an exponential; a power-law fit to the MRX measurements is represented by a dashed $1/x^2$ curve. The power-law prediction is based on a ψ distribution in a 2-D, high Lundquist number ($S>10^4$) model.[50,53] Given these assumptions, it is not surprising that this model is not the best fit for the flux rope half width distribution of the less collisional MRX case. By contrast, a

kinetic description by Fermo *et al.*[51] with a different model for island coalescence predicts an exponential distribution of scale sizes. This model is not only a better fit to the MRX data in Fig. 14 but is also consistent with observations of flux transfer events in the magnetosphere.[51,52] The scale length of the exponential in Fermo *et al.*[51] is a characteristic flux rope scale size; consistent with this, the 2.2 cm scale length of the model in Fig. 14 is similar to the MRX current sheet width. Thus, the similarities between this model and the MRX results suggest a ripe area for further investigations.

An upper bound estimate of the minimum possible size of a small flux rope may be obtained by comparing the Alfvén transit time $\tau_A = L/V_A$ for the structure to move through a layer of length L to the resistive diffusion time $\tau_R = 4\pi w^2/\eta c^2$ over which collisions will smooth out the structure; w represents the structure size. Taking a ratio of these two times

$$\frac{\tau_A}{\tau_R} = \frac{\nu_{ei}}{\Omega_e}\frac{d_i L}{w^2}. \tag{3}$$

An estimate for the minimum structure size based on Eq. (3) is consistent with the experimental results in Fig. 14 and the model of Fermo *et al.*[51] The smallest possible flux rope that can traverse a distance L without dissipating will have τ_A/τ_R of order unity. For typical MRX parameters in the collisionless regime, $\nu_{ei}/\Omega_e \sim 0.02$, $d_i \sim 5$ cm, $L \sim 5$ cm, this gives a minimum scale length $w \sim 0.7$ cm, which cannot be resolved by the fine structure probes. Note that this simple estimate assumes a constant flux rope size and does not consider growth due to reconnection or flux rope merging. Smaller flux ropes could exist transiently and/or grow to a size where resistive diffusion is no longer important. Therefore, 0.7 cm represents an upper bound on the minimum flux rope size. This number is consistent with the model of Fermo *et al.*[51] which states that flux ropes will form due to a tearing instability at scales between the ion and electron skin depths. For the plasma densities of order $\sim 10^{13}/\text{cm}^3$ in the present dataset, the minimum size of 0.7 cm is in this range between the two skin depths.

Also consistent with this estimate, Fig. 14 shows events down to the smallest scale resolved by the probe array. The distribution may fall off below the resistive scale, but this is not possible to show due to limitations in the resolution of the present diagnostics. However, the best available evidence suggests the formation of flux ropes of various sizes as a leading candidate mechanism to prevent the layer from thinning down into ρ_e scales. This modification to the layer structure may render the assumptions used in Dorfman *et al.*[33] to calculate the contribution to the force balance from the off-diagonal pressure terms invalid; however, off-diagonal pressure terms, appropriately modified to consider the small scale structure, may still provide the force balance.

VI. SUMMARY AND CONCLUSIONS

In this paper, impulsive reconnection in MRX is studied in detail, leading to the following three main conclusions:

1. Current layer disruptions are observed in MRX as a fast, impulsive, and *fundamentally three-dimensional* example of magnetic reconnection.
2. Several signatures of flux ropes are identified in the reconnecting current layer. The observed disruptions are due to the buildup and ejection of these 3-D high current density regions associated with O-points at the measurement location.
3. By contrast, magnetic fluctuations, long considered as a possible cause of anomalous resistivity, are not the key physics responsible for the observed impulsive phenomena.

Discharges in MRX are identified in which the reconnection rate peaks and the current in the layer drops suddenly. Important features of this process cannot be explained by 2-D models, suggesting a 3-D, impulsive reconnection process. These "current layer disruptions" are found to be associated with ejection from the reconnection region of high current, O-point structures termed "flux ropes" and a spike in the local reconnection rate. The flux ropes build up in an elongated current layer prior to the disruption in the presence of strong out-of-plane gradients of density and magnetic field. These gradients, found to be present at the start of the discharge pull phase, typically have scale lengths only one order of magnitude greater than that of the field reversal associated with reconnection. During a disruption, the magnetic field gradients flatten on a timescale that may be less than a single ion cyclotron time. The disruption is observed to spread in the electron flow $+y$ direction within the layer. This implies that the observed flux rope structures are ejected from the layer in a 3-D way in both the y and Z (electron flow) directions.

This work was motivated in part by a careful comparison between previous MRX data[27] and 2-D kinetic simulations with well-matched parameters and boundary conditions.[33] The physics matches on the ion scales, but when appropriately normalized to electron scales the thinnest layers in MRX are 3–5 times broader than in the simulations. This discrepancy persists when finite collisions are added to the simulation, and for 3-D simulations in the MRX geometry initialized uniformly in the y direction. This implies that the physics of the electron layers in MRX is inherently three-dimensional. In Roytershteyn *et al.*,[35] magnetic fluctuations are found not to be the cause of these wider electron layers. In the present paper, small scale flux ropes below the probe resolution are proposed as a possible solution.

Electromagnetic fluctuations have long been considered as a source of anomalous resistivity which speeds up the reconnection process.[10,19] A strong correlation is found between the timing of current layer disruptions and the peak in the magnetic fluctuation amplitude in Sec. III. While it is not possible to distinguish cause and effect from the near-simultaneous timing, other features of the disruptions show that they cannot be explained by an anomalous resistivity model. An estimate of the resistivity enhancement in Sec. III due to a wave propagating at the drift speed reveals a contribution far too small to contribute significantly to the out-of-plane force balance. As a result of the disruptive dynamics, E peaks locally while J drops, but this is caused by the

ejection of flux ropes from the layer and is not due to the fluctuations. Out-of-plane gradients, another key feature of disruptions, are also not explained by an anomalous resistivity model. In other words, near the disruption time, conditions are most favorable for the generation of lower hybrid turbulence. The close association of fluctuations and disruptions suggests that the fluctuations may simply be a high frequency component of the disruption dynamics.

In order to explain the observed impulsive behavior, a 3-D, two-fluid model is proposed. The relevant physical picture is an extension of the prior work of Huba and Rudakov,[28] Lapenta *et al.*,[29] Yamada.[12] When there is a gradient in the electron flow velocity v_{ey} due to out-of-plane magnetic field gradients, the resulting electron flow pattern may lead to enhanced reconnection in the y gradient region. The subsequent disruption changes the magnetic field structure in the y gradient region, decreasing the current density. This causes the gradient region to move in the electron flow ($+y$) direction and the disruption spreads in a manner consistent with the "reconnection wave" described by Huba and Rudakov.[28]

An important aspect of this proposed physical picture is that out-of-plane gradients locally drive the reconnection through the Hall term, and the dissipation region adjusts to produce impulsive behavior. This is in direct contrast to anomalous resistivity models where the key physics takes place inside the dissipation region and the outside regions adjust. Thus, this new 3-D two-fluid picture is important because (1) it shows that the Hall terms which leads to steady-state fast reconnection in 2-D can lead to localized, fast, impulsive reconnection in 3-D and (2) it decouples impulsive phenomena from the detailed physics of the electron dissipation region, relegating magnetic fluctuations once thought to be directly responsible for fast reconnection to a less consequential role.

The observations presented in this paper may be particularly applicable to space and astrophysical plasmas where impulsive reconnection occurs. For example, observations of busty bulk flows in the magnetotail are consistent with 3-D bursts of spatially localized reconnection.[54] Other key features of 3-D impulsive reconnection observed in MRX also have possible analogues in space observations, including current disruptions,[55–57] flux rope signatures,[40] and electromagnetic fluctuations.[58,59] Future multi-point satellite studies (e.g., Cluster and MMS) could be used to examine the potential importance of gradients along the X-line. Thus, comparison with MRX observations may provide important clues to the nature of 3-D reconnection processes observed in the magnetotail[22,54] and on the solar surface.[21]

Many opportunities for further investigation remain. Experiments aimed at resolving multiple planes simultaneously in a single discharge are already underway; preliminary results confirm the presence of 3-D flux rope structures. To determine if small-scale flux ropes are continually being generated, construction of probes with finer resolution in the outflow direction is necessary. Some progress has also been made using an active perturbation coil to modify the 3-D structure of the layer; this may shed insight on the initial conditions necessary to trigger disruptive behavior. Such an understanding is especially important to guide future simulation studies; while many simulations see 3-D X-line spreading,[28–32,60] a numerical model that successfully reproduces all the features of an MRX current disruption remains elusive. Also on the simulation side, flux ropes have recently been observed in 3-D MRX simulations in cylindrical geometry; comparison to the results reported here is ongoing. Finally, the many similarities between MRX observations and measurements in the magnetotail suggest the need for a detailed comparison study.

ACKNOWLEDGMENTS

The authors thank W. Daughton and V. Roytershteyn for many insightful discussions and R. Cutler and D. Cylinder for their excellent technical support. S.D. was supported by a DOE FES Fellowship and the NDSEG Fellowship Program. This work was supported in part by the NASA Geospace Science Program grant No. NNH10AO471 and Contract No. DE-AC02-09CH11466 with the US DOE.

[1]M. Yamada, R. Kulsrud, and H. Ji, Rev. Mod. Phys. **82**, 603 (2010).
[2]S. von Goeler, W. Stodiek, and N. Sauthoff, Phys. Rev. Lett. **33**, 1201 (1974).
[3]M. Yamada, F. M. Levinton, N. Pomphrey, R. Budny, J. Manickam, and Y. Nagayama, Phys. Plasmas **1**, 3269 (1994).
[4]B. Kadomtsev, Sov. J. Plasma Phys. **1**, 389 (1975).
[5]E. Parker, *Cosmical Magnetic Fields: Their Origin and Their Activity, International series of monographs on physics* (Clarendon Press, 1979).
[6]S. Tsuneta, Astrophys. J. **456**, 840 (1996).
[7]E. Priest and T. Forbes, *Magnetic Reconnection—MHD Theory and Applications* (Cambridge University Press, 2000).
[8]J. Dungey, Phys. Rev. Lett. **6**, 47 (1961).
[9]J. Birn, *The Dynamic Magnetosphere, IAGA Special Sopron Book Series Vol. 3*, edited by W. Liu, M. Fujimoto, and B. Hultqvist (Springer, The Netherlands, 2011), pp. 49–63.
[10]H. Ji, S. Terry, M. Yamada, R. Kulsrud, A. Kuritsyn, and Y. Ren, Phys. Rev. Lett. **92**, 115001 (2004).
[11]N. Katz, J. Egedal, W. Fox, A. Le, J. Bonde, and A. Vrublevskis, Phys. Rev. Lett. **104**, 255004 (2010).
[12]M. Yamada, Phys. Plasmas **18**, 111212 (2011).
[13]W. Daughton, J. Scudder, and H. Karimabadi, Phys. Plasmas **13**, 072101 (2006).
[14]W. Daughton, V. Roytershteyn, H. Karimabadi, L. K. Yin, B. J. Albright, B. Bergen, and J. Bowers, Nature Phys. **7**, 539 (2011).
[15]R. Davidson and N. Gladd, Phys. Fluids **18**, 1327 (1975).
[16]S. D. Bale, F. S. Mozer, and T. Phan, Geophys. Res. Lett. **29**, 2180, doi:10.1029/2002GL016113 (2002).
[17]T. A. Carter, H. Ji, F. Trintchouk, M. Yamada, and R. M. Kulsrud, Phys. Rev. Lett. **88**, 015001 (2001).
[18]W. Daughton, Phys. Plasmas **10**, 3103 (2003).
[19]Y. Wang, R. Kulsrud, and H. Ji, Phys. Plasmas **15**, 122105 (2008).
[20]E. Priest and T. Forbes, Astron. Astrophys. Rev. **10**, 313 (2002).
[21]P. C. Grigis and A. O. Benz, Astrophys. J. Lett. **625**, L143 (2005).
[22]T. Nagai, J. Geophys. Res. **87**, 4405, doi:10.1029/JA087iA06p04405 (1982).
[23]T. Nagai, I. Shinohara, S. Zenitani, R. Nakamura, T. K. M. Nakamura, M. Fujimoto, Y. Saito, and T. Mukai, J. Geophys. Res. **118**, 1667, doi:10.1002/jgra.50247 (2013).
[24]W. Gekelman and H. Pfister, Phys. Fluids **31**, 2017 (1988).
[25]E. E. Lawrence and W. Gekelman, Phys. Rev. Lett. **103**, 105002 (2009).
[26]T. P. Intrator, X. Sun, G. Lapenta, L. Dorf, and I. Furno, Nature Phys. **5**, 521 (2009).
[27]Y. Ren, Ph.D. dissertation, Princeton University, 2007.
[28]J. D. Huba and L. I. Rudakov, Phys. Plasmas **9**, 4435 (2002).
[29]G. Lapenta, D. Krauss-Varban, H. Karimabadi, J. D. Huba, L. I. Rudakov, and P. Ricci, Geophys. Res. Lett. **33**, L10102, doi:10.1029/2005GL025124 (2006).

[30]L. S. Shepherd and P. A. Cassak, J. Geophys. Res.: Space Phys. **117**, A10101 (2012).
[31]L. I. Rudakov and J. D. Huba, Phys. Rev. Lett. **89**, 095002 (2002).
[32]J. D. Huba and L. I. Rudakov, Phys. Plasmas **10**, 3139 (2003).
[33]S. Dorfman, W. Daughton, V. Roytershteyn, H. Ji, Y. Ren, and M. Yamada, Phys. Plasmas **15**, 102107 (2008).
[34]V. Roytershteyn, W. Daughton, S. Dorfman, Y. Ren, H. Ji, M. Yamada, H. Karimabadi, L. Yin, B. J. Albright, and K. J. Bowers, Phys. Plasmas **17**, 055706 (2010).
[35]V. Roytershteyn, S. Dorfman, W. Daughton, H. Ji, M. Yamada, and H. Karimabadi, Phys. Plasmas **20**, 061212 (2013).
[36]M. Yamada, H. Ji, S. Hsu, T. Carter, R. Kulsrud, N. Bretz, F. Jobes, Y. Ono, and F. Perkins, Phys. Plasmas **4**, 1936 (1997).
[37]Y. Ren, M. Yamada, S. Gerhardt, H. Ji, R. Kulsrud, and A. Kuritsyn, Phys. Rev. Lett. **95**, 055003 (2005).
[38]Y. Ren, M. Yamada, H. Ji, S. Dorfman, S. P. Gerhardt, and R. Kulsrud, Phys. Plasmas **15**, 082113 (2008).
[39]T. D. Tharp, A. F. Almagri, M. C. Miller, V. V. Mirnov, S. C. Prager, J. S. Sarff, and C. C. Kim, Phys. Plasmas **17**, 120701 (2010).
[40]J. P. Eastwood, T.-D. Phan, F. S. Mozer, M. A. Shay, M. Fujimoto, A. Retinò, M. Hesse, A. Balogh, E. A. Lucek, and I. Dandouras, J. Geophys. Res. **112**, A06235, doi:10.1029/2006JA012158 (2007).
[41]M. Inomoto, S. P. Gerhardt, M. Yamada, H. Ji, E. Belova, A. Kuritsyn, and Y. Ren, Phys. Rev. Lett. **97**, 135002 (2006).
[42]S. Dorfman, H. Ji, M. Yamada, J. Yoo, E. Lawrence, C. Myers, and T. D. Tharp, Geophys. Res. Lett. **40**, 233, doi:10.1029/2012GL054574 (2013).
[43]O. Buneman, Phys. Rev. **115**, 503 (1959).
[44]T. Tange and S. Ichimaru, J. Phys. Soc. Jpn. **36**, 1437 (1974).
[45]NRC, *Plasma Physics of the Local Cosmos* (The National Academies Press, 2004).
[46]P. A. Cassak, M. A. Shay, and J. F. Drake, Phys. Rev. Lett. **95**, 235002 (2005).
[47]W. Daughton, V. Roytershteyn, B. J. Albright, H. Karimabadi, L. Yin, and K. J. Bowers, Phys. Plasmas **16**, 072117 (2009).
[48]E. Harris, Il Nuovu Cimento **23**, 115 (1962).
[49]S. Dorfman, Ph.D. dissertation, Princeton University, 2012.
[50]D. A. Uzdensky, N. F. Loureiro, and A. A. Schekochihin, Phys. Rev. Lett. **105**, 235002 (2010).
[51]R. L. Fermo, J. F. Drake, and M. Swisdak, Phys. Plasmas **17**, 010702 (2010).
[52]R. L. Fermo, J. F. Drake, M. Swisdak, and K.-J. Hwang, J. Geophys. Res. **116**, A09226, doi:10.1029/2010JA016271 (2011).
[53]Y.-M. Huang and A. Bhattacharjee, Phys. Rev. Lett. **109**, 265002 (2012).
[54]M. A. Shay, J. F. Drake, M. Swisdak, W. Dorland, and B. N. Rogers, Geophys. Res. Lett. **30**, 1345, doi:10.1029/2002GL016267 (2003).
[55]A. T. Y. Lui, A. Mankofsky, C.-L. Chang, K. Papadopoulos, and C. S. Wu, Geophys. Res. Lett. **17**, 745, doi:10.1029/GL017i006p00745 (1990).
[56]S. Ohtani, K. Takahashi, L. J. Zanetti, T. A. Potemra, R. W. McEntire, and T. Iijima, J. Geophys. Res. **97**, 19311, doi:10.1029/92JA01832 (1992).
[57]D. N. Baker, T. I. Pulkkinen, V. Angelopoulos, W. Baumjohann, and R. L. McPherron, J. Geophys. Res. **101**, 12975, doi:10.1029/95JA03753 (1996).
[58]J. S. Pickett, J. R. Franz, J. D. Scudder, J. D. Menietti, D. A. Gurnett, G. B. Hospodarsky, R. M. Braunger, P. M. Kintner, and W. S. Kurth, J. Geophys. Res. **106**, 19081, doi:10.1029/2000JA003012 (2001).
[59]M. Zhou, X. H. Deng, S. Y. Li, Y. Pang, A. Vaivads, H. Rème, E. Lucek, S. Fu, X. Lin, Z. G. Yuan *et al.*, J. Geophys. Res. **114**, A02216, doi:10.1029/2008JA013427 (2009).
[60]Jain *et al.*, Phys. Plasmas **20**, 112101 (2013).

The Princeton Plasma Physics Laboratory is operated
by Princeton University under contract
with the U.S. Department of Energy.

Information Services
Princeton Plasma Physics Laboratory
P.O. Box 451
Princeton, NJ 08543

Phone: 609-243-2245
Fax: 609-243-2751
e-mail: pppl_info@pppl.gov
Internet Address: http://www.pppl.gov